Available online at www.sciencedirect.com
SCIENCE DIRECT®
Journal of Solid State Chemistry 177 (2004) 3290–3300
JOURNAL OF SOLID STATE CHEMISTRY
http://elsevier.com/locate/jssc

Valence and structural transitions in the mixed Ru–Ir perovskites $Ba_2PrRu_{1-x}Ir_xO_6$

Leqing Li and Brendan J. Kennedy*

Center for Heavy Metals Research, School of Chemistry, The University of Sydney, Sydney NSW 2006, Australia

Received 11 December 2003; received in revised form 2 May 2004; accepted 12 May 2004

Available online 20 July 2004

Abstract

The valence state of Pr in the *B*-site ordered double perovskites $Ba_2PrRu_{1-x}Ir_xO_6$ is shown to be sensitive to both the precise Ru:Ir content and temperature. Pr L_{III} XANES measurements show that at room temperature the Pr is trivalent in the Ru-rich compounds with $x<0.25$. At higher Ir contents the Pr is tetravalent. High-resolution powder synchrotron X-ray and neutron diffraction methods have been used to study the composition and temperature dependence of the crystal structures of these oxides. The Ru and Ir are statistically distributed on one of the two available *B*-sites. The oxides undergo an apparently first-order monoclinic $P2_1/n$ to tetragonal $P4/mnc$ phase transition in response to the change on the Pr and Ru/Ir valence. High temperatures and Ru contents favor the lower symmetry monoclinic structure, that is arises from the presence of the larger Pr^{III} cations. The variations in the observed metal–oxygen bond distances are consistent with a simultaneous change in the valence of the Ru/Ir accompanying the Pr^{III}–Pr^{IV} valence transition.

Keywords: Valence transition; Metal oxides; Structure; Neutron diffraction

1. Introduction

The crystal structures and magnetic properties of ruthenium and iridium perovskites have been extensively studied over the past 20 years [1–5] with much of this interest being directed towards the ternary or double perovskites of the type $ABB'O_6$ [6–15]. The term double perovskite is commonly used to describe *B*-site ordered perovskites of the general formulae $A_2BB'O_6$. The Ru and Ir double perovskites have the general form A_2LnMO_6 where A = Ca, Sr, Ba, Ln = Y, La or a lanthanide and M = Ru or Ir where the Ln and M-type cations have a rock-salt like ordering within the perovskite-like cell [16,17]. In A_2LnRuO_6 perovskites the Ru is generally present as Ru^V. The d^3 Ru^V ions are antiferromagentically coupled and these oxides exhibit complicated low temperature magnetic behavior. The analogous Ir compounds also display interesting magnetic properties which, when M = Ce, Tb or Pr, indicate that the lanthanide ion and Ir are both in the +4 oxidation state.

Recently Wakeshima et al. [18] described the preparation, crystal structures and magnetic properties of ordered double perovskites in the series $Ba_2PrRu_{1-x}Ir_xO_6$. This system is particularly interesting since the oxidation state of Pr and M (Ru or Ir) are different in the two end members. Therefore there exists the possibility of observing a transition between these two valence levels. Wakeshima et al. [18] reported that single-phase samples were observed at low $0.0\leqslant x\leqslant 0.05$ and high $0.55\leqslant x\leqslant 1.0$ Ru contents but that at intermediate compositions $0.1\leqslant x\leqslant 0.5$ the samples contained two double perovskite phases. They concluded that the Ru-rich oxides were of the form $Ba_2Pr^{3+}(Ru,Ir)^{5+}O_6$ and the Ir rich compounds were $Ba_2Pr^{4+}(Ru,Ir)^{4+}O_6$. At intermediate compositions these two phases co-existed.

Whilst there are a number of examples of intermetallic compounds that switch valence levels in response to changes in composition, temperature or pressure [19–25] there are considerably fewer examples of valence transitions in metal oxides. One notable exception is $TlReO_4$ where the Tl ion changes its valence from Tl^+ to Tl^{3+} and Re from Re^{7+} to Re^{5+} in resonse to changes in either temperature or pressure [26]. In metal oxides

*Corresponding author. Fax: +61-2-9351-3329.
E-mail address: kennedyb@chem.usyd.edu.au (B.J. Kennedy).

0022-4596/$ - see front matter © 2004 Elsevier Inc. All rights reserved.
doi:10.1016/j.jssc.2004.05.033

valence transitions are more commonly observed as valence averaging, for example the formally Fe(IV) in the orthorhombic perovskite $CaFeO_3$ disproportionates to the valence ordered $Ca_2Fe^{V}Fe^{III}O_6$ monoclinic structure at low temperatures [27]. Here the valence transition induces a structural phase transition as a consequence of the difference in the size of the iron cation in the three oxidation states. In other oxides such as $BaBiO_3$ [28] and $CsAuCl_3$ [29] only the valence ordered state is stable and there is no evidence for valence averaging. The structure of the valence ordered $Ca_2Fe^{V}Fe^{III}O_6$ phase is the same as that found in Ba_2PrRuO_6 [30] and proposed to exist across the entire $Ba_2PrRu_{1-x}Ir_xO_6$ series [18]. It would be surprising if the valence transition in these perovskites was not accompanied by a structural phase transition.

In general it is possible to estimate the oxidation state of a metal ion in an oxide through an examination of the M–O bond distances, higher oxidation states have smaller average M–O distances. This can be quantified using methods such as bond valence sum calculations. An alternate approach is to directly measure the energy of an electronic transition involving metal based orbitals that are sensitive to the oxidation state of the metal. X-ray absorption near edge spectroscopy (XANES) is such a method.

It has been shown that XANES is capable of providing information on the valence of Ru, Ir and Pr cations [31–36]. In the present context Pr L_{III} edge XANES is potentially very useful since it is reported that the edge shift in going from trivalent Pr to tetravalent Pr is nearly three times that seen in going from Ru^{IV} to Ru^{V} and Ir^{IV} to Ir^{V}. The appearance of the XANES can also provide information on the symmetry and oxidation state of the absorbing ion.

In the present study, we report the results of a high-resolution powder diffraction study for the solid solution $Ba_2PrRu_{1-x}Ir_xO_6$ ($0.0 \leqslant x \leqslant 1.0$). Both synchrotron X-ray and neutron diffraction methods have been used to determine the structures of these oxides. Pr L_{III} XANES spectroscopy has been used to investigate the valence of the Pr in these oxides. In agreement with Wakeshima et al. [18] we find evidence for a discontinuity in the structure at compositions near $x = 0.3$. We show that this is a consequence of a first-order monoclinic–tetragonal structural phase transition associated with a Pr^{III}–Pr^{IV} valence transition.

2. Experimental

2.1. Sample preparation

Polycrystalline samples of 15 members in the series $Ba_2PrRu_{1-x}Ir_xO_6$, with $x = 0.0$, 0.05, 0.10, 0.15, 0.20, 0.25, 0.30, 0.35, 0.40, 0.50, 0.60, 0.70, 0.80, 0.90, 1.00, were synthesized by solid-state reaction of barium carbonate, ruthenium metal, iridium metal and praseodymium oxide, each with a purity of more than 99.9%. The required stoichiometric quantities were ground, pressed into pellets and calcined in air at 1173 K for 48 h. The calcined materials were then reground, pelletized and sintered in air at 1473 K for 5 days with several intermediate regrinding and re-pelletizing steps.

2.2. XANES measurement

Pr L_{III}-edge XANES spectra were collected in transmission mode at the ANBF on Beamline 20B at the KEK Photon Factory, Japan [37]. The samples were diluted in boron nitride (~15% by weight) to give the optimum signal to noise ratio. The samples were finely ground and evenly packed into 1-mm thick aluminum cells with Kapton tape windows. During the measurements the synchrotron operated at 2.5 GeV with a maximum stored current of 450 mA. The beam line is equipped with a Si (111) channel cut monochromator. All Pr L_{III}-edge XANES were recorded using a step width of 0.25 eV and a counting time of 3 s per data point at room temperature. $PrAlO_3$ and $BaPrO_3$ were chosen to provide Pr^{III} and Pr^{IV} reference spectra.

2.3. Synchrotron X-ray diffraction measurement

High-resolution synchrotron X-ray diffraction patterns were recorded using the 530-mm Debye-Scherrer diffractometer on Beamline 20B at the Photon Factory [37]. This instrument uses image plates (IP) as detectors, each Fuji 20×40 cm IP covering a 2θ angular range of 40°. The data were collected in 0.01° angular steps using 0.75117 Å X-rays. The samples were housed in rotating 0.3-mm-diameter capillaries. For the room temperature measurements data were collected using three IPs covering an angular range of 5–125°. Variable-temperature synchrotron X-ray diffraction patterns were recorded for $Ba_2PrRu_{0.5}Ir_{0.5}O_6$ and $Ba_2PrRu_{0.6}Ir_{0.4}O_6$ using a custom-built furnace. These data were collected using two IPs covering an angular range of 5–85°. The structural refinements were carried out using the program Rietica [38] where the instrumental parameters were refined using a Voigt profile function. The data from the individual IPs were treated as separate histograms in the refinements, with the instrumental and profile parameters for each histogram constrained to be equal. In all cases the background of the lowest angle histogram was estimated by interpolation of up to 40 points and the background in the high angle histograms was defined by a third-order polynomial in 2θ, the parameters for which were refined simultaneously with the other structural and profile parameters.

2.4. Neutron diffraction measurement

Neutron powder diffraction patterns for $Ba_2PrRu_{0.7}Ir_{0.3}O_6$ were recorded using thermal neutrons with wavelength of 1.4925 Å over the range $5° < 2\theta < 155°$ in 0.05° steps on the HRPD at ANSTO [39]. Data were collected at temperatures between 100 and 400 K. The sample (~10 g) was lightly ground and was contained in a thin-walled vanadium can. The background was defined by a third-order polynomial in 2θ in the Rietveld refinements.

3. Results and discussion

The powder synchrotron X-ray diffraction patterns for the series of the double perovskites $Ba_2PrRu_{1-x}Ir_xO_6$ showed that single-phase samples were obtained for both low $0.0 \leqslant x \leqslant 0.25$ and high $0.50 \leqslant x \leqslant 1.0$ Ir contents, Fig. 1. At intermediate compositions all the observed reflections were clearly split and it was concluded that the samples with composition $0.30 \leqslant x \leqslant 0.40$ contained two phases. These observations are similar to those in Table 1 of Wakeshima et al. [18]. The small differences possibly reflect the different preparative conditions used in the two studies. Examination of the profile for Ba_2PrRuO_6 showed a weak 1 1 1 (in $Fm3m$) reflection near $2\theta = 8.8°$as a result of cation ordering. Rietveld refinements of the structures for the Ru rich oxides with $x < 0.25$ were then undertaken in the monoclinic space group $P2_1/n$. This structural type was observed in a recent high-resolution powder neutron diffraction study by Izumiyama et al. [30]. The refined structural parameters for Ba_2PrRuO_6, Table 1, are in good agreement with those reported in this recent neutron diffraction study [30]. Very similar results were obtained for all the Ru rich single-phase samples. Attempts to use this model for the single-phase Ir rich samples proved more difficult. It was found that the refinements tended to be unstable when the monoclinic β angle was refined, this oscillating either side of 90°. Further the refined lattice parameters were consistent with a tetragonal metric. The appropriateness of tetragonal symmetry for the Ir rich samples was verified by comparing the results of Le Bail-type analysis in both possible symmetries [38]. These two observations prompted us to consider the possibility that the symmetry of the Ir rich compounds was higher than monoclinic.

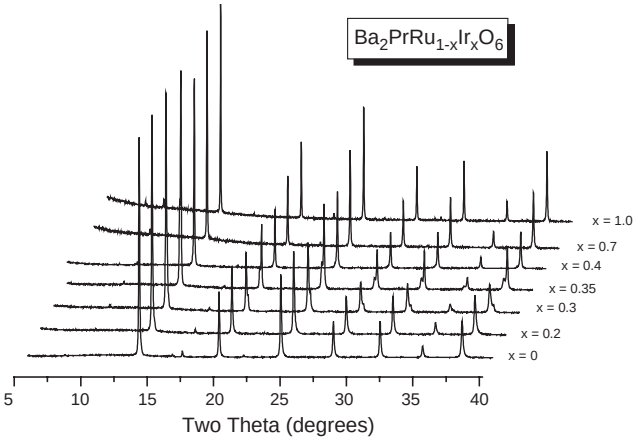

Fig. 1. Portions of the synchrotron X-ray diffraction patterns for $Ba_2PrRu_{1-x}Ir_xO_6$ with $x = 0$, 0.2, 0.3, 0.35, 0.4, 0.7, 1.0 recorded at $\lambda = 0.75117$ Å.

The monoclinic structure seen in Ba_2PrRuO_6 is derived from that of the basic perovskite by the co-existence of rock-salt like ordering of the cations and tilting of the MO_6 octahedra [16,17,40]. In the absence

Table 1
Structural parameters for Ba_2PrRuO_6 and Ba_2PrIrO_6 at room temperature, refined from synchrotron powder X-ray diffraction data

Atom	x	y	z	Biso
Ba_2PrRuO_6 space group $P2_1/n$				
Ba	0.0040(6)	0.0046(4)	0.2481(6)	1.27(2)
Pr	0.5	0	0	1.48(3)
Ru	0.5	0	0.5	0.55(2)
O1	0.200(4)	0.269(4)	−0.015(3)	0.2(1)
O2	0.227(5)	−0.288(4)	−0.014(4)	0.2(1)
O3	−0.019(5)	0.525(3)	0.236(3)	0.2(1)
$a = 6.0049(2)$, $b = 5.9912(2)$, $c = 8.4914(3)$ Å, $\beta = 90.02(1)°$, $R_p = 4.95$, $R_{wp} = 6.29\%$				
Ba_2PrIrO_6 space group $P4/mnc$				
Ba	0	0	0	0.48(1)
Pr	0	0	0	0.23(1)
Ir	0.5	0	0	0.11(1)
O1	0	0	0.262(4)	0.6(2)
O2	0.243(2)	0.716(3)	0	0.6(2)
$a = 5.9395(1)$, $c = 8.4007(2)$ Å, $R_P = 3.03$, $R_{WP} = 3.67\%$				

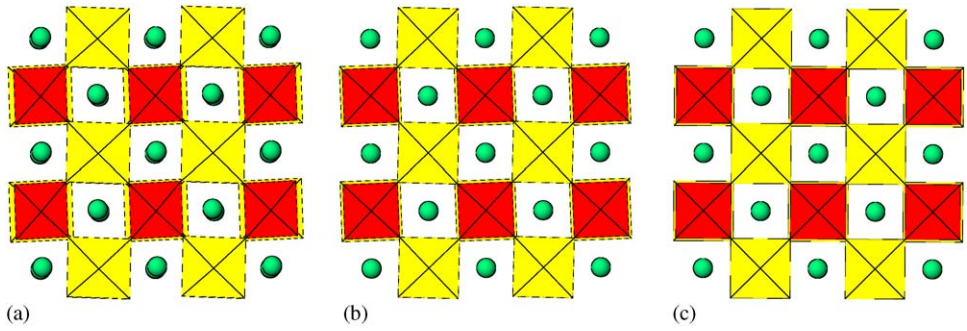

Fig. 2. Representation of the ideal *Fm*3*m* cubic double perovskite structure and that of the tetragonal *P*4/*mnc* and monoclinic $P2_1/n$ structures. The structural parameters obtained for $Ba_2PrRu_{0.7}Ir_{0.3}O_6$ at 100 and 400 K were used to draw the tetragonal and monoclinic structures, respectively. The tilting and size of the PrO_6 octahedra is clearly larger in the high temperature monoclinic structure.

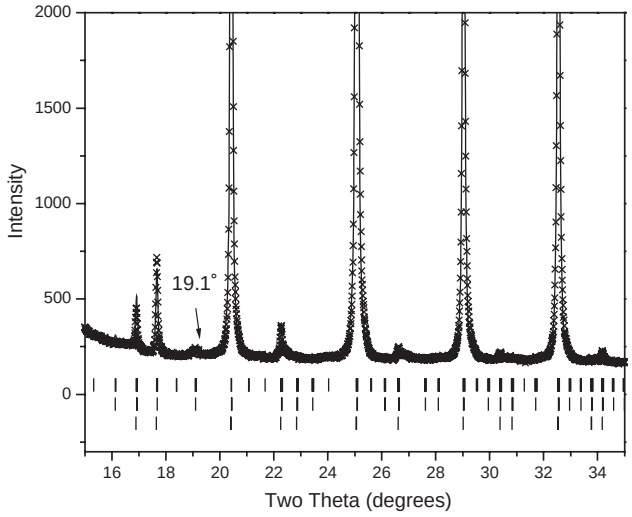

Fig. 3. Section of the Rietveld profiles for Ba_2PrRuO_6 in region 15–35° recorded using synchrotron X-rays with $\lambda = 0.75117$ Å. The structure has been fitted in space group $P2_1/n$. The upper set of vertical lines shows the positions of the Bragg reflections allowed in $P2_1/n$. The middle set show those allowed in *P*4/*mnc* and the lower lines are those in *I*4/*m*. The observed superlattice peak around 19.1° is allowed by $P2_1/n$ and *P*4/*mnc* but prohibited by *I*4/*m*.

of such tilting the ideal double structure is cubic in space group $Fm\bar{3}m$ with $a_{DP} \approx 2a_p$, where *a* is the unit cell length of the double perovskite (DP) or perovskite (*P*). Following the notation introduced by Glazer [41] both in-phase (+) and out-of-phase (−) tilts of the MO_6 octahedra are present in the monoclinic Ba_2PrRuO_6 structure. The tilt system in $P2_1/n$ is described as $a^- a^- c^+$. As for the simple ABO_3 perovskites these tilts arise from a mismatch in the size of the *A*- and *M*-type cations. The magnitude of the tilts, their axis and type (in or out-of-phase) will be sensitive to the relative sizes of the cations.

A group theoretical analysis was then undertaken with the aid of the computer program ISOTROPY [42] in order to identify possible space groups in the double perovskites. Full details of this analysis are given elsewhere [40]. From this it was concluded that transitions involving the removal of a tilt from $P2_1/n$ to *P*4/*mnc* or *I*4/*m* were equally possible. These three structures are on the same volume $(\sqrt{2}a \times \sqrt{2}b \times 2c)$ cell but differ in the nature of the tilting of the MO_6 octahedra. *I*4/*m* ($a^0a^0c^-$) has only out-of-phase tilts *P*4/*mnc* ($a^0b^+b^+$) only in-phase tilts and $P2_1/n$ both in- and out-of-phase tilts. The structures in both *P*4/*mnc* and $P2_1/n$ are shown in Fig. 2, highlighting the out-of-phase tilts. As is evident from this figure (which is generated using refined atomic coordinates for $Ba_2PrRu_{0.7}Ir_{0.3}O_6$) the out-of-phase tilts are reasonably small in both structures. The symmetry allows the PrO_6 and Ru/IrO_6 rotations to be unequal in $P2_1/n$ and we find these to be small $<2°$, and within the precision of the refinements, equal. As illustrated in Fig. 3 there are relatively few reflections allowed in $P2_1/n$ that are extinct in *P*4/*mnc*. In the present case all these reflections are calculated to have zero intensity in the X-ray diffraction profiles of the monoclinic compounds including Ba_2PrRuO_6 itself. This compound is undoubtedly monoclinic [30]. Clearly then the systematic absence of these reflections cannot be used to distinguish between $P2_1/n$ and *P*4/*mnc*. Rather, we have relied on the cell metric and Rietveld analysis to distinguish between these. The second possible tetragonal structure identified is *I*4/*m*. This space group has been seen in numerous double perovskites including Sr_2FeMoO_6 and Ba_2CuWO_6 [43,44]. The diffraction pattern for Ba_2PrRuO_6 shows a number of weak reflections violating I-centering, showing *I*4/*m* to be incorrect. We observe that these reflections systematically weakened as the Ir content increased, Fig. 4. Critically some of these reflections were observed in $Ba_2PrRu_{0.6}Ir_{0.4}O_6$, which is beyond the region where the monoclinic model was appropriate. We have followed the usual procedure of assigning the highest possible symmetry that is consistent with the data. Based on the observed tetragonal metric for these cells the structures of the Ir rich $x > 0.4$

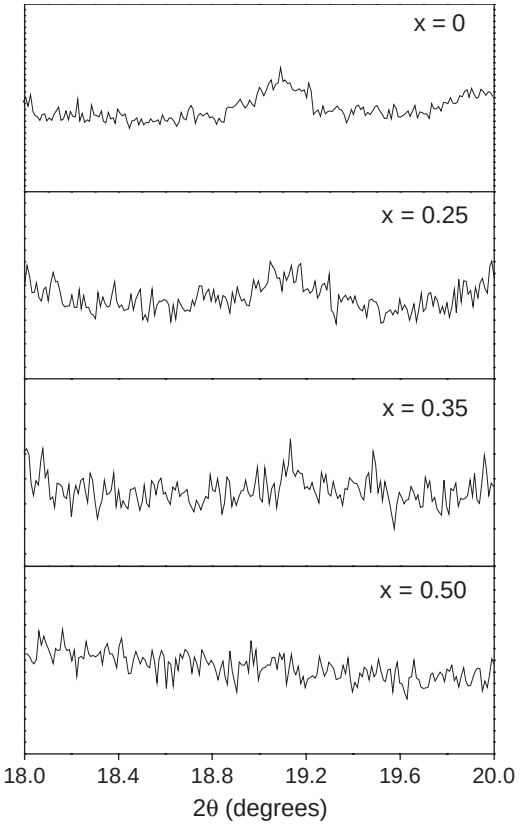

Fig. 4. Portions of the synchrotron X-ray diffraction patterns for $Ba_2PrRu_{1-x}Ir_xO_6$ with $x=0$, 0.25, 0.35, and 0.5 showing the progressive weakening of the superlattice peak at around 19.1°. This reflection is only present when $x \leqslant 0.4$ and is no longer observed at higher Ir contents.

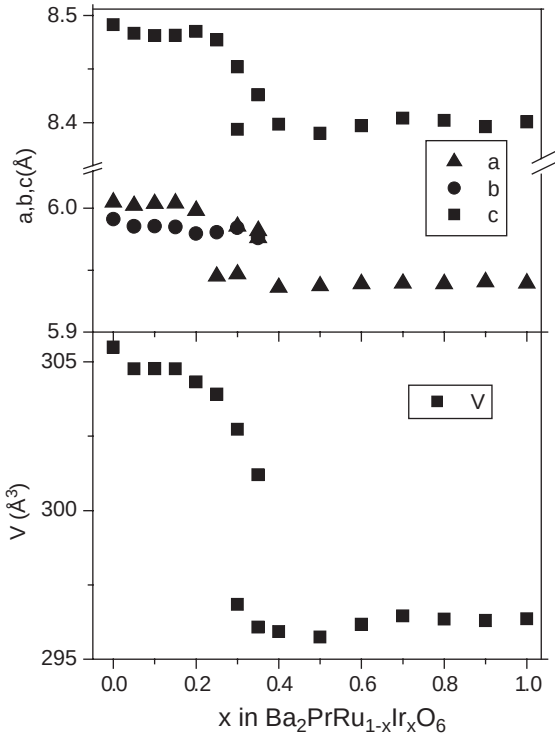

Fig. 5. Variation of the unit cell parameters, cell volumes distances in the series $Ba_2PrRu_{1-x}Ir_xO_6$.

oxides were then refined in *P*4/*mnc*. In all cases the refinements proved satisfactory and the atomic coordinates for Ba_2PrIrO_6 are listed in Table 1.

Next the profiles for the samples with intermediate compositions $x = 0.30$ and 0.35 were examined using a two-phase $P2_1/n$ and *P*4/*mnc* model in which the Ru:Ir ratio for the two phases was constrained to be equal. As described in more detail below, variable temperature diffraction measurements showed the two phases to be in thermal equilibrium and so we concluded that this region corresponds to the co-existence of the two phases in equilibrium, rather than a composition induced miscibility gap. Based on both the variation in the lattice parameters and the persistence of a *P*-type cell at compositions with $x > 0.25$ we concluded that a first-order $P2_1/n$ to *P*4/*mnc* transition occurs near $x = 0.25$ at room temperature. We propose that the tetragonal *P*4/*mnc* structure persists over the composition range $0.30 \leqslant x \leqslant 1.0$, Fig. 5. The refined lattice parameters for the 15 compositions studied are given in Table 2.

In order to verify that the two-phase region is a consequence of co-existence of the two phases being in equilibrium with each other this we examined the temperature dependence of the structures of three samples using either powder neutron or X-ray diffraction methods. The synchrotron X-ray studies showed that at room temperature $Ba_2PrRu_{0.7}Ir_{0.3}O_6$ is composed of a major $P2_1/n$ and minor *P*4/*mnc* phases. This was also observed in a neutron powder diffraction pattern recorded at 280 K, Fig. 6 and the successful Rietveld analysis of this pattern required the presence of both the monoclinic $P2_1/n$ and tetragonal *P*4/*mnc* phases. The larger sample volume required for the neutron diffraction measurements compared to the synchrotron diffraction measurements means that the former is much less susceptible to local inhomogeneities. As the temperature was lowered to 100 K the amount of the monoclinic phase present decreased and the Rietveld analysis showed that the sample consisted of only the tetragonal *P*4/*mnc* phase at or below 220 K. Conversely, heating the sample above room temperature resulted in a progressive decrease in the amount of the tetragonal phase present and a single $P2_1/n$ phase was obtained at or above 380 K, Fig. 7. Examples of the Rietveld refinement for the *P*4/*mnc* phase model at 100 K, the $P2_1/n$ phase model at 380 K, the two phases model at 280 K are shown in Fig. 6. A summary of all the refinements from the neutron diffraction data for $Ba_2PrRu_{0.7}Ir_{0.3}O_6$ is given in Table 3, whilst Table 4 gives fuller details at two selected temperatures, 100 and 400 K. Izumiyama and co-workers recently studied the magnetic structure of Ba_2PrRuO_6 using powder neutron diffraction and reported that this remains monoclinic

Table 2
Lattice parameters and cell volumes of $Ba_2PrRu_{1-x}Ir_xO_6$ at room temperature

X	Space group	a (Å)	b (Å)	c (Å)	β	V (Å^3)
0.00	$P2_1/n$	6.0049(2)	5.9912(2)	8.4914(3)	90.02(1)	305.49(4)
0.05	$P2_1/n$	6.0022(3)	5.9853(3)	8.4833(5)	90.09(1)	304.76(2)
0.10	$P2_1/n$	6.0037(2)	5.9854(2)	8.4812(4)	89.98(1)	304.77(4)
0.15	$P2_1/n$	6.0041(3)	5.9848(3)	8.4813(4)	89.96(1)	304.76(4)
0.20	$P2_1/n$	5.9981(3)	5.9794(3)	8.4852(5)	90.13(1)	304.32(4)
0.25	$P2_1/n$	5.9806(2)	5.9945(2)	8.4771(3)	90.08(1)	303.91(4)
0.30	$P2_1/n$	5.9853(4)	5.9841(5)	8.4521(5)	89.79(1)	302.73(4)
	P4/mnc	5.9469(3)	5.9470(3)	8.3938(6)		296.86(4)
0.35	$P2_1/n$	5.9760(3)	5.9818(3)	8.4259(5)	89.67(1)	301.20(4)
	P4/mnc	5.9357(2)		8.4035(4)		296.08(4)
0.40	*P4/mnc*	5.9360(2)		8.39834)		295.93(6)
0.50	*P4/mnc*	5.9372(2)		8.3900(5)		295.75(6)
0.60	*P4/mnc*	5.9389(2)		8.3972(6)		296.17(5)
0.70	*P4/mnc*	5.9393(1)		8.4042(3)		296.46(5)
0.80	*P4/mnc*	5.9390(2)		8.4020(3)		296.35(6)
0.90	*P4/mnc*	5.9405(2)		8.3963(5)		296.30(3)
1.00	*P4/mnc*	5.9395(1)		8.4007(2)		296.36(4)

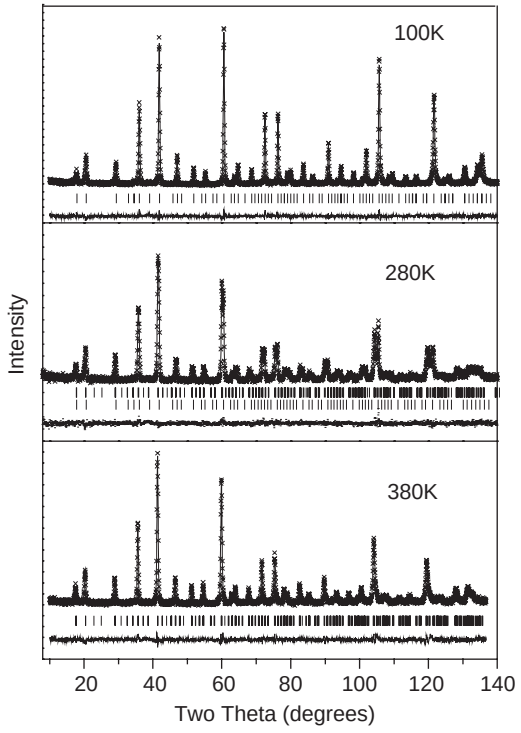

Fig. 6. Rietveld profiles for $Ba_2PrRu_{0.7}Ir_{0.3}O_6$ at 100, 280 and 380 K from the 1.4925 Å neutron diffraction data. The structure has been fitted in *P4/mnc* at 100 K, $P2_1/n$ at 380 K and as a two-phase mixture at 280 K.

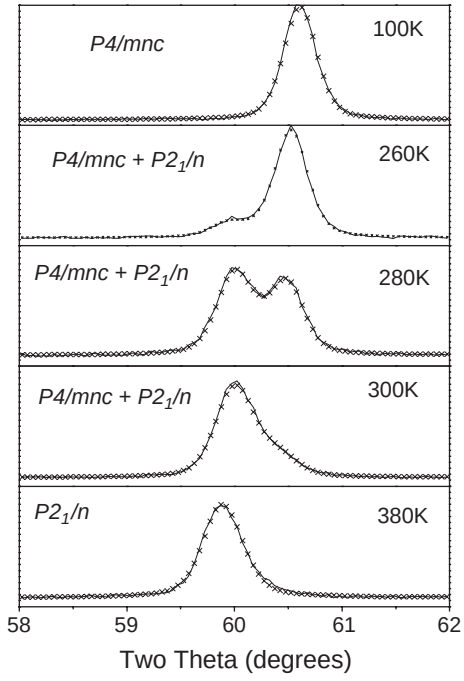

Fig. 7. Portions of the neutron Rietveld profiles for $Ba_2PrRu_{0.7}Ir_{0.3}O_6$ at temperatures between 100 and 380 K showing the transition from the tetragonal to monoclinic structures.

down to the lowest temperature studied, 7 K [30]. When assuming monoclinic symmetry we could not get stable refinements for $Ba_2PrRu_{0.7}Ir_{0.3}O_6$ using the low temperature neutron diffraction data, even when constraining the cell metric to be tetragonal, presumably as a consequence of too much freedom in the oxygen positional parameters. No such problems were found when the structure was refined in the tetragonal structure.

The temperature dependence of the cell parameters, unit cell volume and average bond lengths for $Ba_2PrRu_{0.7}Ir_{0.3}O_6$ are shown in Fig. 8. All these show an obvious discontinuity near 240 K indicative of a first-order phase transition. The co-existence of the monoclinic and tetragonal structures is consistent with this.

Table 3
Temperature-dependent lattice parameters and cell volumes of $Ba_2PrRu_{0.7}Ir_{0.3}O_6$

Temp (K)	Space group	a (Å)	b (Å)	c (Å)	β	V (Å^3)
100	$P4/mnc$	5.9285(5)		8.3866(13)		294.76(6)
140	$P4/mnc$	5.9301(5)		8.3878(13)		294.96(7)
160	$P4/mnc$	5.9306(5)		8.3893(13)		295.06(6)
180	$P4/mnc$	5.9309(6)		8.3931(16)		295.23(6)
200	$P4/mnc$	5.9322(4)		8.3912(11)		295.29(7)
220	$P4/mnc$	5.9331(6)		8.3939(16)		295.48(7)
240	$P4/mnc$	5.9360(5)		8.3920(14)		295.70(6)
260	$P4/mnc$	5.9377(6)		8.3982(18)		296.09(7)
280	$P4/mnc$	5.9406(5)		8.402(4)		296.5(3)
	$P2_1/n$	5.9844(12)	5.9896(12)	8.449(2)	90.22(1)	302.8(1)
300	$P4/mnc$	5.947(2)		8.404(6)		297.2(2)
	$P2_1/n$	5.980(2)	5.986(3)	8.465(3)	90.09(3)	303.0(2)
320	$P4/mnc$	5.9638(12)		8.395(2)		298.58(11)
	$P2_1/n$	5.983(2)	5.988(2)	8.469(2)	90.05(3)	303.3(2)
340	$P4/mnc$	5.9649(13)		8.407(2)		299.11(12)
	$P2_1/n$	5.986(2)	5.991(2)	8.466(3)	90.04(2)	303.6(2)
360	$P4/mnc$	5.965(2)		8.404(2)		299.09(14)
	$P2_1/n$	5.986(2)	5.993(2)	8.467(3)	90.03(2)	303.7(2)
380	$P4/mnc$	5.967(2)		8.408(2)		299.40(13)
	$P2_1/n$	5.985(2)	5.9939(12)	8.475(3)	90.07(2)	304.0(2)
400	$P2_1/n$	5.987(3)	5.992(2)	8.476(3)	90.09(3)	304.1(2)

Table 4
Structural parameters for $Ba_2PrRu_{0.7}Ir_{0.3}O_6$ at 100 and 400 K refined from powder neutron diffraction data

Atom	x	y	z	Biso	N
$Ba_2PrRu_{0.7}Ir_{0.3}O_6$ 100 K					
Ba	0	0.5	0.25	0.31(3)	0.250
Ru	0	0	0	0.32(5)	0.087
Ir	0	0	0	0.32(5)	0.038
Pr	0	0	0.5	0.33(9)	0.125
O1	0	0	0.236(1)	-0.1(1)	0.250
O2	0.237(2)	0.761(2)	0	0.82(8)	0.500
$a = 5.9300(5)$, $c = 8.382(1)$ Å, R_p6.72, R_{wp}7.96%					
$Ba_2PrRu_{0.7}Ir_{0.3}O_6$ 400 K					
Ba	0.484(9)	0.505(6)	0.2405(99)	0.6(2)	1.00
Pr	0	0.5	0	0.5(2)	0.500
Ru	0.5	0	0	0.6(1)	0.350
Ir	0.5	0	0	0.6(1)	0.150
O1	0.275(7)	0.255(10)	0.009(5)	1.7(8)	1.000
O2	0.269(9)	0.775(10)	0.007(5)	0.3(9)	1.000
O3	0.502(7)	-0.001(6)	0.233(7)	2.0(8)	1.000
$a = 5.986(4)$, $b = 5.992(2)$, $c = 8.478(4)$ Å, β90.08(3)°, R_p6.90, R_{wp}8.52%					

Interestingly these show that increasing the temperature results in a transition to the higher volume, but lower symmetry, cell. This contrasts with the results seen in simple perovskites such as $SrRuO_3$ [3] where increasing the temperature increases the symmetry through the removal of the RuO_6 tilts. A similar first-order transition to a lower symmetry cell is observed on heating $LaGaO_3$ [45]. The neutron studies demonstrate that the two-phase mixture observed at room temperature can be converted to a single-phase sample by either heating and cooling demonstrating the two phases to be in thermal equilibrium. We note that the volume of the tetragonal phase is noticeably larger in the two-phase region (between 275 and 350 K) than seen in the single-phase lower temperature region. Whilst the volume is expected to increase as the temperature increases, the observed change is somewhat larger than expected and may indicate fluctuation in the valence levels prior to the phase transition.

The synchrotron diffraction pattern for $Ba_2PrRu_{0.6}Ir_{0.4}O_6$ at room temperature shows this to be single phase and tetragonal. Heating this to near 775 K results in the appearance of additional strong reflections and the patterns recorded between 775 and 850 K

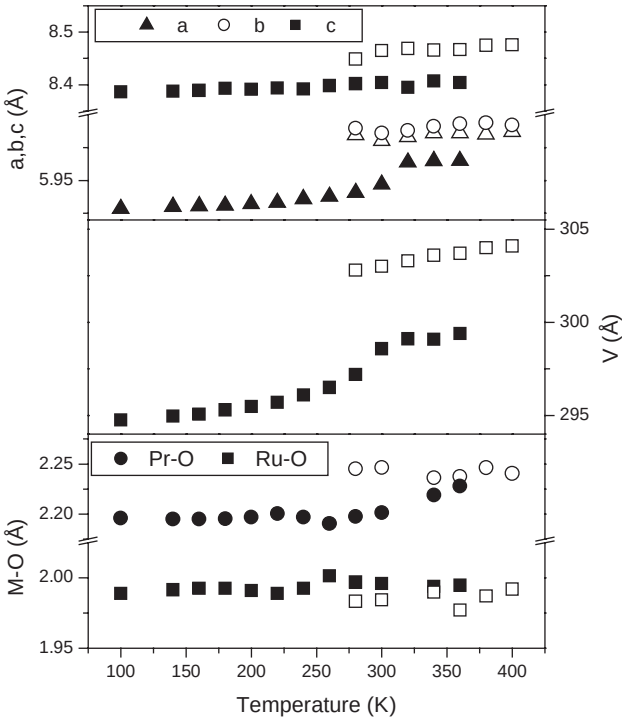

Fig. 8. Temperature dependence of the unit cell parameters, cell volumes and M–O distances in $Ba_2PrRu_{0.7}Ir_{0.3}O_6$. The discontinuity near 260 K is a consequence of the first-order phase transition. The closed symbols are represent values for the tetragonal structures and the open symbols those for the monoclinic structures.

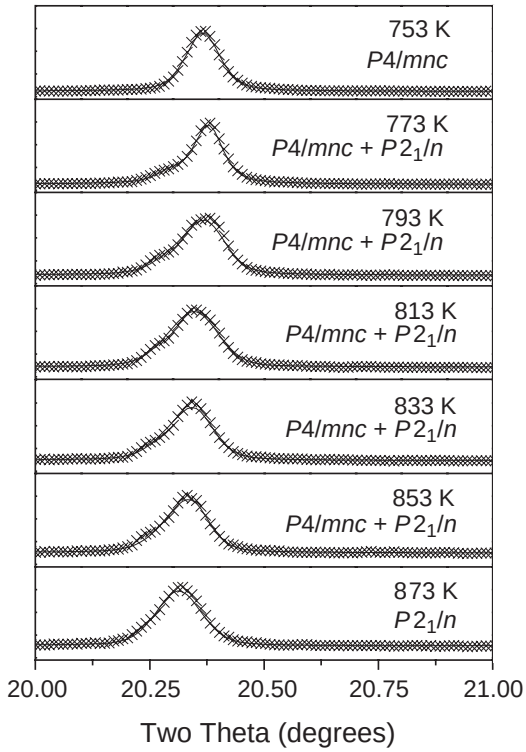

Fig. 9. Portions of the synchrotron Rietveld profiles for $Ba_2PrRu_{0.6}Ir_{0.4}O_6$ at temperatures between 750 and 875 K showing the transition from the tetragonal to monoclinic structures.

indicate of a two-phase mixture, Fig. 9. Further heating this sample then results in the formation of a single, monoclinic, phase. These assignments were confirmed by Rietveld analysis. Heating a sample of tetragonal $Ba_2PrRu_{0.5}Ir_{0.5}O_6$ to near 1075 K resulted in the formation of a small amount of a monoclinic phase, co-existing with the tetragonal phase. Presumably heating this to still higher temperatures would result in the complete transition to the monoclinic phase.

The cell volumes of the monoclinic structure are clearly larger that those of the tetragonal phase in both the composition and temperature dependent studies, Figs. 5 and 8. Wakeshima et al. [18] noted a similar change, although they did not identify the change in symmetry apparent in our higher resolution studies. Since the ionic radii of Ru and Ir, in the same oxidation state, are approximately equal it might be expected that the volumes of the solid solutions would be independent of the Ru:Ir ratio. Experimentally this is not observed, rather the complexes apparently exist in two series. However the volumes of the members within each of these two series are approximately constant. As noted above in Ba_2PrIrO_6 the Ir is present as Ir^{IV}. If Ir^{IV} progressively replaces the Ru^{V}, as $Ba_2Pr^{3+}Ru^{5+}_{1-x}Ir^{4+}_{x}O_6$, then it would be necessary to either have partial oxidation of the Pr^{3+} or to introduce oxygen vacancies to maintain charge neutrality. The structural refinements from the neutron diffraction data show no evidence for any oxygen non-stiochiometry in $Ba_2PrRu_{0.7}Ir_{0.3}O_6$. Furthermore Ir^{4+} is larger than Ru^{5+} and it is unlikely that a contraction in the cell volume caused by the introduction of oxygen vacancies (one is required for every two Ir^{IV} ions added) would be sufficient to offset the expansion in the cell volume induced by the larger cation.

Since experimentally the cell volume is observed to show a discontinuous decrease upon the addition of Ir to Ba_2PrRuO_6 a smaller cation must be introduced. The only available smaller cation is Pr^{4+}. This suggests that the composition, including oxidation states, may be written as $Ba_2Pr^{3+}_{1-x}Pr^{4+}_{x}Ru^{5+}_{1-x}Ir^{4+}_{x}O_6$. Alternatively it may be that as a consequence of the increase in the M–O bond lengths as Ir^{4+} is added to the system the Ru^{5+} is reduced to Ru^{4+} with the Pr^{3+} being oxidized to Pr^{4+} so that the composition of the Ir rich compounds is actually $Ba_2Pr^{4+}Ru^{4+}_{1-x}Ir^{4+}_{x}O_6$. The present data does not allow us to unambiguously distinguish between these two possibilities. Another possible explanation, that the Pr is oxidized to Pr^{4+} without reduction of the Ru (or Ir), appears unlikely based on charge neutrality.

The observed changes in the average M–O distances seen in both the room temperature composition dependence studies and the variable temperature powder neutron diffraction study indicate a first-order phase

transition. Both above and below the critical point the average M–O distances are reasonably constant suggesting the oxidation state of the constituent ions to be constant in the two regions. The relative decrease in ionic radii in going from Pr^{3+} to Pr^{4+} (0.14 Å) is much larger than the rate of increase for M^{5+} (M = Ru, Ir) to M^{4+} (0.055 Å) [18,46]. Therefore a valence transition of the type $Ba_2Pr^{3+}M^{5+}O_6$ to $Ba_2Pr^{4+}M^{4+}O_6$ is expected to result in a contraction in the cell volume, since the volume of the PrO_6 octahedron should decrease much more rapidly than the increase in the volume of the MO_6 octahedron. Examination of the volumes of the PrO_6 and MO_6 octahedra in the high and low-temperature phases of $Ba_2PrRu_{0.7}Ir_{0.3}O_6$ demonstrates this to be the case. The volumes for the PrO_6 octahedra increasing from 14.2 $Å^3$ at 100 K to 15.6 $Å^3$ at 400 K whereas that of the MO_6 octahedra remains essentially constant over the same temperature range 10.6–10.2 $Å^3$. These volume changes are evident on examination of the two structures with the high temperature $P2_1/n$ structure having the larger PrO_6 octahedra and the more distorted structure than the low temperature $P4/mnc$ structure, Fig. 2.

Following Teraoka [47] we have estimated the fitness factor, Ω, for the two valence states where $\Omega = \sqrt{2}r_A/(r_B + r_O)$ with r_A is the radii of the A-type cation, r_B the average radii of the two B-type cations and r_O the radii of the oxygen anion [46]. We find the fitness factor for the Pr^{4+}/M^{4+} state $\Omega = 0.974$ is higher than that for the Pr^{3+}/M^{5+} state $\Omega = 0.957$. Teraoka et al. [47] proposed that the fitness factor is a more sensitive measure of the tendency for double perovskites to adopt a distorted structure than the more usual tolerance factor. They concluded that higher values of Ω favor higher symmetry structures. The conclusion that the tetragonal structure is the Pr^{4+}/M^{4+} state is consistent with this analysis.

In order to confirm the valence changes described above Pr L_{III} XANES have been recorded for selected samples. The composition dependence of the Pr L_{III} XANES for the series $Ba_2PrRu_{1-x}Ir_xO_6$ at room temperature is illustrated in Fig. 10. Analysis of these spectra did not reveal a clear edge. Focussing on the region near 5965 eV we note that the relatively complex spectra observed for the Ir rich samples with $0.4 \leqslant x \leqslant 0.9$ becomes somewhat simpler in the Ru rich compounds with $x < 0.3$. In particular the features near 5973 eV are absent in these Ru rich compounds. The change in peak shape near $x = 0.3$ is believed to indicate of a change in Pr valence. The spectra obtained for the pure Ir oxide Ba_2PrIrO_6 is clearly anomalous and is worthy of a more detailed investigation. A pseudo-doublet white line in the Pr L_{III} edge XANES is characteristic of tetravalent Pr and is observed in oxides such as PrO_2 and $BaPrO_3$. The two peaks arise from excited many-body final states. The peak at higher

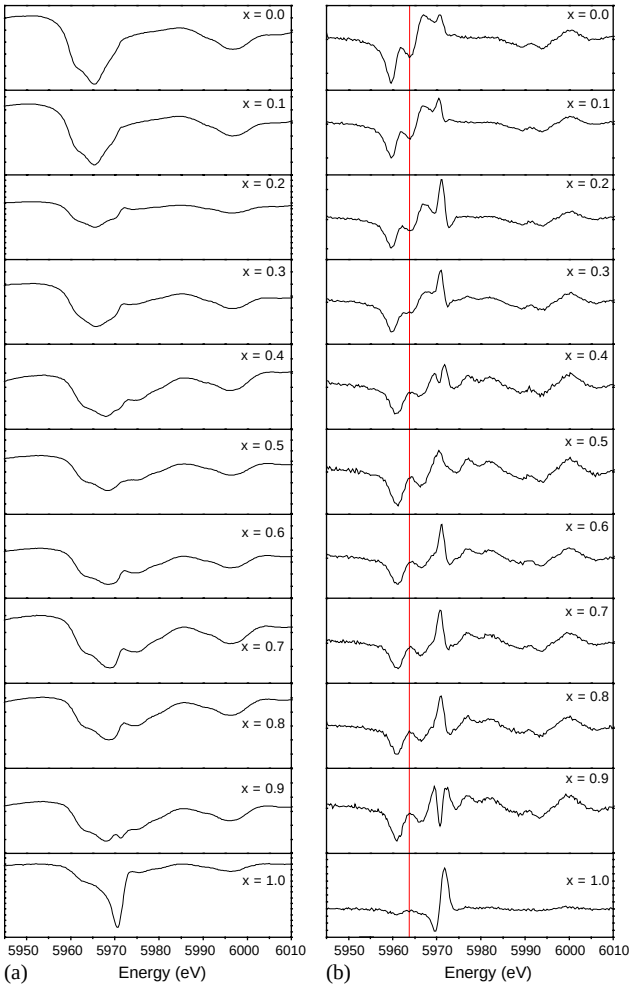

Fig. 10. The (a) Pr-L_{III} XANES spectra and (b) their first derivatives for $Ba_2PrRu_{1-x}Ir_xO_6$ ($x = 0$, 0.1, 0.2, 0.3, 0.4, 0.5, 0.6, 0.7, 0.8, 0.9, 1.0). The vertical line highlights the position of the feature diagnostic for Pr^{IV}.

energy is assigned to essentially a core-excited Pr^{3+} final state with the configuration $2p4f15d^*$; here, $2p$ denotes a hole in the $2p$ shell (with $J = 3/2$), while $5d^*$ refer to the excited electron in the $5d$ state. The peak at lower energy corresponds mainly to a charge transfer final state $2p4f25d^*L$, where L stands for a hole in the anion orbitals [31,32]. On the other hand, the L_{III} edge spectra of many trivalent Pr compounds including PrF_3 [33] and Pr_2BaO_4 [31] exhibit a single resonance peak. This single peak is sometimes split [31] due to the hybridization. The change in peak shape near $x = 0.3$ may be indicative of a change in the Pr valence state.

Examination of the derivatives of the Pr L_{III} XANES is equally informative. There is a feature near 5964 eV in the Ru rich oxides that shifts abruptly to near 5966 eV as the Ir content is increased to $x > 0.4$. This feature is noticeably poorly resolved in the $x = 0.3$ sample, which the diffraction measurements have shown to contain two phases, and presumably a mixture of Pr^{III} and Pr^{IV}

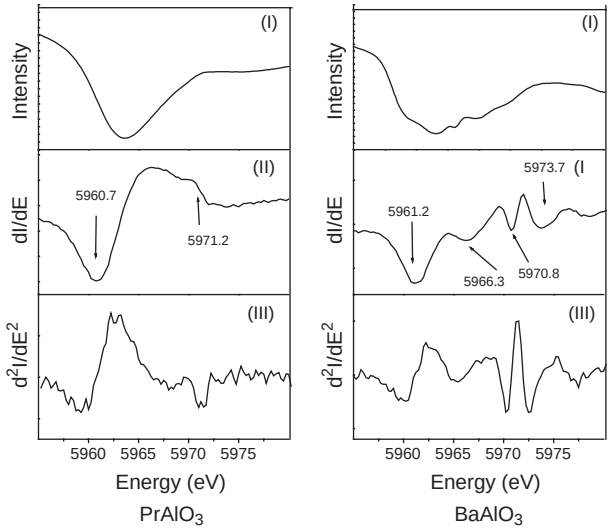

Fig. 11. Observed (I) and first (II) and second (III) derivative Pr L_{III} XANES for $PrAlO_3$ and $BaPrO_3$.

cations. We observe a similar minimum in the first derivative of the Pr L_{III} XANES for the Pr^{IV} standard $BaPrO_3$. This is not observed for the Pr^{III} standard $PrAlO_3$. It is possible that the absence of a comparable feature in the XANES of $PrAlO_3$ is a consequence of the geometry, Fig. 11. Although both standards are perovskites in $PrAlO_3$ the Pr^{III} occupies the 12-coordinate *A*-type perovskite site, whereas in $BaPrO_3$ the Pr^{IV} occupies the 6-coordinate *B*-type site. This 6-coordinate geometry is the same, as that found for Pr in the present double perovskites. Furthermore the Ir rich oxides display, in the first derivative trace, a feature near 2974.5 eV that is also observed in the Pr^{IV} standard $BaPrO_3$ but not in the Pr^{III} standard $PrAlO_3$. We conclude that the XANES are consistent with a change in the valence from Pr^{III} in the Ru rich compounds with $x<0.3$ to Pr^{IV} in the Ir rich compounds with $x\geqslant 0.4$. The further studies of L_{III}-edge XANES of Ru and Ir which can provide information on the valence state of these cations [34–36] would be useful.

4. Conclusions

We have shown that the first-order transition in the series $Ba_2PrRu_{1-x}Ir_xO_6$ is a consequence of a valence transition of the type $Ba_2Pr^{III}M^{V}O_6$ to $Ba_2Pr^{IV}M^{IV}O_6$. The Pr L_{III} edge XANES shows that at high Ru contents $x\leqslant 0.2$ the Pr is in the trivalent state whereas at low Ru contents $x\geqslant 0.4$ tetravalent Pr is present. The smaller size of Pr^{IV} relative to that of Pr^{III} induces a structural transition from monoclinic $P2_1/n$ to tetragonal. Analysis of the diffraction patterns shows the presence of reflections in the tetragonal phase that violates I-centering. The most likely space group for the tetragonal phase is $P4/mnc$. Altering the temperature induces the same transition. Whereas in simple perovskites such as $CaTiO_3$ [48] or $SrRuO_3$ [3] increasing the temperature favors the higher symmetry structure in this case higher temperatures favor the lower symmetry monoclinic structure. Neutron and/or electron diffraction studies to confirm the symmetry of the Ir rich compounds would be useful.

Acknowledgments

The Australian Research Council supported this work. The Australian Institute of Nuclear Science Engineering supported the neutron diffraction measurements. The synchrotron measurements at the Australian National Beamline Facility were supported by the Australian Synchrotron Research Program, which is funded by the Commonwealth of Australia under the Major National Research Facilities program. We thank Drs. James Hester and Garry Foran for their assistance with these measurements and Dr. C.J. Howard for his ongoing interest in this work.

References

[1] J.J. Randall, R. Ward, J. Am. Chem. Soc. 81 (1959) 2629.
[2] H.W. Schmalle, C. Gurtner, H.R. Oswald, A. Reller, Z. Kristallogr. 191 (1990) 239.
[3] B.J. Kennedy, B.A. Hunter, J.R. Hester, Phys. Rev. B 65 (2002) 224103.
[4] C.W. Jones, P.D. Battle, P. Lightfoot, W.T.A. Harrison, Acta Crystallogr. C 45 (1989) 365.
[5] T. Kiyama, K. Yoshimura, K. Kosuge, Y. Ikeda, Y. Bando, Phys. Rev. B 54 (1996) R756.
[6] P.D. Battle, Mater. Res. Bull. 16 (1981) 397.
[7] P.D. Battle, J.B. Goodenough, J. Price, J. Solid State Chem. 46 (1983) 234.
[8] P.D. Battle, W.J. Macklin, J. Solid State Chem. 52 (1984) 138.
[9] N.G. Parkinson, P.D. Hatton, J.A.K. Howard, C. Ritter, F.Z. Chien, M.K. Wu, J. Mater. Chem. 13 (2003) 1468.
[10] Y. Doi, Y. Hinatsu, A. Nakamura, Y. Ishii, Y. Morii, J. Mater. Chem. 13 (2003) 1758.
[11] H.A. Blackstead, J.D. Dow, D.R. Harshman, W.B. Yelon, M.X. Chen, M.K. Wu, D.Y. Chen, F.Z. Chien, D.B. Pulling, Phys. Rev. B 63 (2001) 214412.
[12] Y. Izumiyama, Y. Doi, M. Wakeshima, Y. Hinatsu, A. Nakamura, Y. Ishii, J. Solid State Chem. 169 (2002) 125.
[13] Y. Doi, Y. Hinatsu, K. Oikawa, K.Y. Shimojo, Y. Morii, J. Alloys, Compounds 323 (2001) 455.
[14] Y. Doi, Y. Hinatsu, K. Oikawa, K.Y. Shimojo, Y. Morii, J. Mater. Chem. 10 (2000) 797.
[15] Y. Doi, Y. Hinatsu, K. Oikawa, K.Y. Shimojo, Y. Morii, J. Mater. Chem. 10 (2000) 1731.
[16] M.T. Anderson, K.B. Greenwood, G.A. Taylor, K.R. Poeppelmeir, Prog. Solid State Chem. 22 (1993) 197.
[17] R.H. Mitchell, Perovskites: Modern and Ancient, Almaz Press, Ontario Canada, 2002.
[18] M. Wakeshima, Y. Izumiyama, Y. Doi, Y. Hinatsu, Solid State Commun. 120 (2001) 273.

[19] J.M. Lawrence, P.S. Riseborough, R.D. Parks, Rep. Prog. Phys. 44 (1981) 1.
[20] A. Jayaraman, V. Narayanamurti, E. Bucher, R.G. Maines, Phys. Rev. Lett. 25 (1970) 1430.
[21] J.L. Sarrao, A.P. Ramirez, T.W. Darling, F. Freibert, A. Migliori, C.D. Immer, Z. Fisk, Y. Uwatoko, Phys. Rev. B 58 (1998) 409.
[22] D.T. Adroja, B.D. Rainford, J.M. de Teresa, A. del Moral, M.R. Ibarra, K.S. Knight, Phys. Rev. B 52 (1995) 12790.
[23] T. Takabatake, F. Teshima, H. Fujii, S. Nishigori, T. Suzuki, T. Fujita, Y. Yamaguchi, J. Sakurai, D. Jaccard, Phys. Rev. B 41 (1990) 9607.
[24] W. Zhang, N. Sato, K. Yoshimura, A. Mitsuda, T. Goto, K. Kosuge, Phys. Rev. B 66 (2002) 024112.
[25] H. Wada, M.F. Hundley, R. Movshovich, J.D. Thompson, Phys. Rev. B 59 (1999) 1141.
[26] A. Jayaraman, G.A. Kourouklis, L.G. Van Uitert, Phys. Rev. B 36 (1987) 8547.
[27] P.M. Woodward, D.E. Cox, E. Moshopoulou, A.W. Sleight, S. Morimoto, Phys. Rev. B 62 (2000) 844.
[28] D.E. Cox, A.W. Sleight, Acta Crystallogr. B 35 (1979) 1.
[29] P. Day, C. Vettier, G. Parisot, Inorg. Chem. 17 (1978) 2319.
[30] Y. Izumiyama, Y. Doi, M. Wakeshima, Y. Hinatsu, Y. Shimojo, Y. Morii, J. Phys.: Condens. Matter 13 (2001) 1303.
[31] J. Dumschat, G. Wortmann, I. Felner, Physica B 209 (1995) 313.
[32] E. Alleno, C. Godart, B. Fisher, J. Genossar, L. Patlagan, G.M. Reisner, Physica B 261 (1999) 531.
[33] U. Staub, L. Soderholm, S.R. Wasserman, A.G.O. Conner, M.J. Kramer, B.D. Patterson, M. Shi, M. Knapp, Phys. Rev. B 61 (2000) 1548.
[34] J.H. Choy, J.Y. Kim, S.H. Hwang, S.J. Kim, G. Demazeau, Int. J. Inorg. Mater. 2 (2000) 61.
[35] Z. Hu, H. von Lips, M.S. Golden, J. Fink, G. Kaindl, F.M.F. de Groot, S. Ebbinghaus, A. Reller, Phys. Rev. B 61 (2000) 5262.
[36] J.H. Choy, D.K. Kim, S.H. Hwang, G. Demazeau, D.Y. Jung, J. Am. Chem. Soc. 117 (1995) 8557.
[37] T.M. Sabine, B.J. Kennedy, R.F. Garrett, G.J. Foran, D.J. Cookson, J. Appl. Crystallogr. 28 (1995) 513.
[38] C.J. Howard, B.A. Hunter, A Computer Program for Rietveld Analysis of X-ray and Neutron Powder Diffraction Patterns, Lucas Heights Research Laboratories, 1998, pp. 1–27.
[39] C.J. Howard, C.J. Ball, R.L. Davis, M.M. Elcombe, Aust. J. Phys. 36 (1983) 507.
[40] C.J. Howard, B.J. Kennedy, P.M. Woodward, Acta Crystallogr. B 59 (2003) 463.
[41] A.M. Glazer, Acta Crystallogr. B 28 (1972) 3384;
A.M. Glazer, Acta Crystallogr. B 31 (1975) 756.
[42] ISOTROPY available from www.physics.byu.edu/~stokesh/isotropy.html
[43] O. Chmaissem, R. Kruk, B. Dabrowski, D.E. Brown, X. Xiong, S. Kolesnik, J.D. Jorgensen, C.W. Kimball, Phys. Rev. B 62 (2000) 14197.
[44] Bokhimi, Powder Diffraction 7 (1992) 228.
[45] B.J. Kennedy, C.J. Howard, J. Phys. C: Condens. Matter 11 (1999) 3229.
[46] R.D. Shannon, Acta Crystallogr. Sect. A 32 (1976) 751.
[47] Y. Teraoka, M.D. Wei, S. Kagawa, J. Mater. Chem. 8 (1998) 2323.
[48] B.J. Kennedy, C.J. Howard, B.C. Chakoumakos, J. Phys. C: Condens. Matter 11 (1999) 1479.